RESEARCH ARTICLE OPEN ACCESS

Design and Evaluation of Performance Characteristics of a 2kw Small Scale Horizontal Axis Wind Turbine Blade Using Analytical and Numerical Approaches

Supreeth R*, S K Maharana**

*(Research Scholar, Department of Aeronautical Engineering, Acharya Institute of Technology, Bengaluru supreethr@rvce.edu.in)

** (Dean and Head, Department of Aeronautical Engineering, Acharya Institute of Technology, Bengaluru skmaha123@gmail.com)

----------**********----------

Abstract:

Small scale horizontal axis wind turbines are few of the last mile solutions for power generation in rural areas disconnected from the grid. Wind turbines with efficient blade design can be implemented in regions with sub-optimal wind velocities for maximum power extraction. In the study here, with the aid of Blade Element Momentum theory an efficient blade for a 2kW small scale wind turbine is developed. Later, the performance of the linearized blade in terms of torque Q and power coefficient $C_p$at various wind velocities U_∞ and Tip Speed Ratios λ are estimated through k−ω SST turbulence model available in ANSYS® FLUENT software. Comparison of the outcomes obtained through BEM and ANSYS software shows that the torque Q and power coefficient $C_p$achieved through simulation are matching well with the BEM results. The outcomes also promise the combination of BEM theory and linearization technique in achieving a simple yet highly capable blade.

Keywords **—Renewable Energy, Small Scale Wind Turbines, Wind Energy**

----------**********----------

I. INTRODUCTION

A wind turbine is complex machinery consisting of several parts working in unison with an objective to convert the kinetic energy from the oncoming wind into useful electrical energy [1]. From component perspective, a typical horizontal axis wind turbine will include the blade, hub, nacelle, generator, tower, nose cone, tail. With increase in the size of the turbine blade, the wind turbine system will invariably lead to sophistication upon the addition of some components like drive train, gear box, drive shaft, braking system, pitch control systems, yawing system, electrical generator, heat exchangers, balancing system and many more [2] [3]. Though wind turbine is composed of several individualistic components, the most critical one that severely affects the energy transfer process is the blade. Blade is the dynamic component that directly interacts with the free stream wind. The maximum power generated depends on the aerodynamic profiling of the blade. Since, blades forms the critical component, the underlying study encompasses the design of a blade for a small scale horizontal axis wind turbine blade.

Highly efficient wind turbines can extract around 59% of the energy available from the wind [4]. Experimental investigations show that the theoretical maximum efficiency of a wind turbine operating under realistic environment will never outperform Betz limit, unless the tip speed and lift-drag ratios approach infinity [5]. From an extensive study, the blade planform, blade airfoil, number of

blades and the tip speed ratio are of paramount importance influencing the aerodynamic output of a wind turbine [6]. To maximise the energy output, the airfoils with highest cl/cd ratio needs to be selected [7, 8, 9].Additionally combination of thick and thin airfoils will generally yield a blade that is structurally and aerodynamically sound [10]. Furthermore, combination of S822 and S823 airfoils is highly employable for stall regulated wind turbine blades due to its reduced weight, increased stiffness and finally the restrained C_{lmax} augments the annual yield of the turbines. Gur et al. [11] proposed the importance of incorporating the influence of drag coefficient and tip losses for simulating real world environment. Consideration of Tip loss factor is imperative in predicting the actual performance of a wind turbine under real working conditions [12]. Experiments performed by Giguère at al. [13] highlighted the provision of linear taper and nonlinear twist to be beneficial in maximizing the annual energy production of the wind turbine. [14] designed a wind turbine blade for 10kW operating at design velocity and tip speed ratio of 10m/s and 6 respectively. The numerical results of the blade performance obtained using combined RANS and Spalart-Allmaras turbulence model were satisfactorily validated with the aid of Blade Element Momentum theory. Additionally, the prediction of wind turbine blade performance can be numerically achieved through RANS turbulence model which proves to be in good agreement with the BEM theory as investigated in [15].

As highlighted in the literature section, a key aspect that directly affects the energy output of a wind turbine is the airfoil underlying the blade of a turbine. In this study efforts are made to understand the performance characteristics of the rotor blade composed of S823 and S822 airfoils. The blades developed for 2k W fixed pitch fixed speed wind turbine will be analyzed for wind velocities U_∞=1-20m/s and tip speed ratio λ=1-20 using Blade Element Momentum theory. Next, the performance of the rotor blade will be ascertained through k–ω SST turbulence model available in ANSYS® FLUENT simulation software and the results will be validated with the BEM theory.

II. ANALYTICAL STUDIES

A. Blade Element Momentum Theory

Traditionally, BEM theory is implemented for design of rotor blades for wind turbines irrespective of the scale of operation. BEM theory has been dedicatedly developed by blending momentum theory and blade element theory, known as strip theory. The BEM theory enumerated in [3] is followed for designing and analytically investigating the performance of the blade. The various steps involved in BEM theory is schematically represented by figure 1.

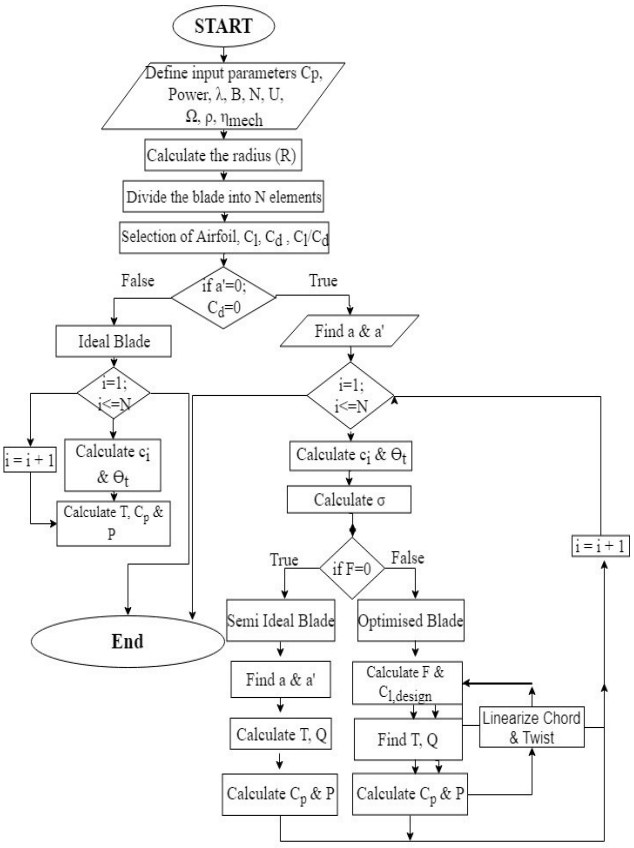

Fig.1 Schematic of Blade Element Momentum Theory for designing of wind turbine blades

B. Geometric and Operating parameters of the Blade

Primary objective of the study is to design and analyze the performance of a rotor blade for a power output P = 2kW at design conditions. For

the specified operating conditions, the radius of the blade can be ascertained through the Eq.1.

$$P = \frac{1}{2}\rho\pi R^2 U^3 C_p \eta \quad (1)$$

In Eq.1, P is the rated power (2kW), ρ is the air density (1.23k g/m^3), U is the Design wind velocity (10m/s), C_P is the Power coefficient (0.45) and η being the generator efficiency (0.90). The radius of the blade works out to be R = 1.60m for the stated operating conditions.

C. Airfoils and their aerodynamic properties

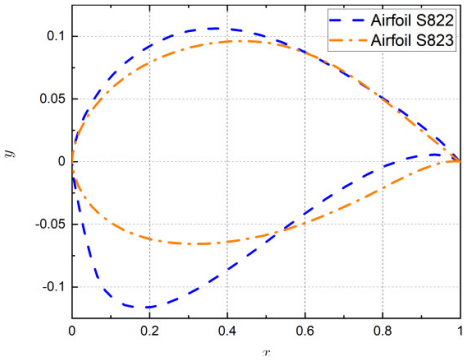

Fig.2 Geometric profiles of S823 and S822 airfoils used for the blade

TABLE 1

AERODYNAMIC CHARACTERISTICS OF S822 AND S823 AIRFOILS

Blade Station	Airfoil	Geometrical Properties		Aerodynamic Characteristics at Re=100000		
		Max Thickness	Max Camber	C_{lmax}	C_{dmin}	C_l/C_d
0.1R-0.3R	S823	21.2% at 24.3%c	2.4% at 70.5%c	1.157 at 15^0	0.02842 at 9.25^0	42.23 at 9.25^0
0.35R-1R	S822	1 6% at 39.2% c	1.8% at 59.5% c	0.926 at 13^0	0.02190 at 8.5^0	42.69 at 8.5^0

Based on the literature, NREL S822 and S823 airfoils shown in figure 3a are considered. Further, the aerodynamic characteristics of S823 and S822 airfoils at Re=100000 are provided in table 1 and the aerodynamic curves are presented in figure 3.

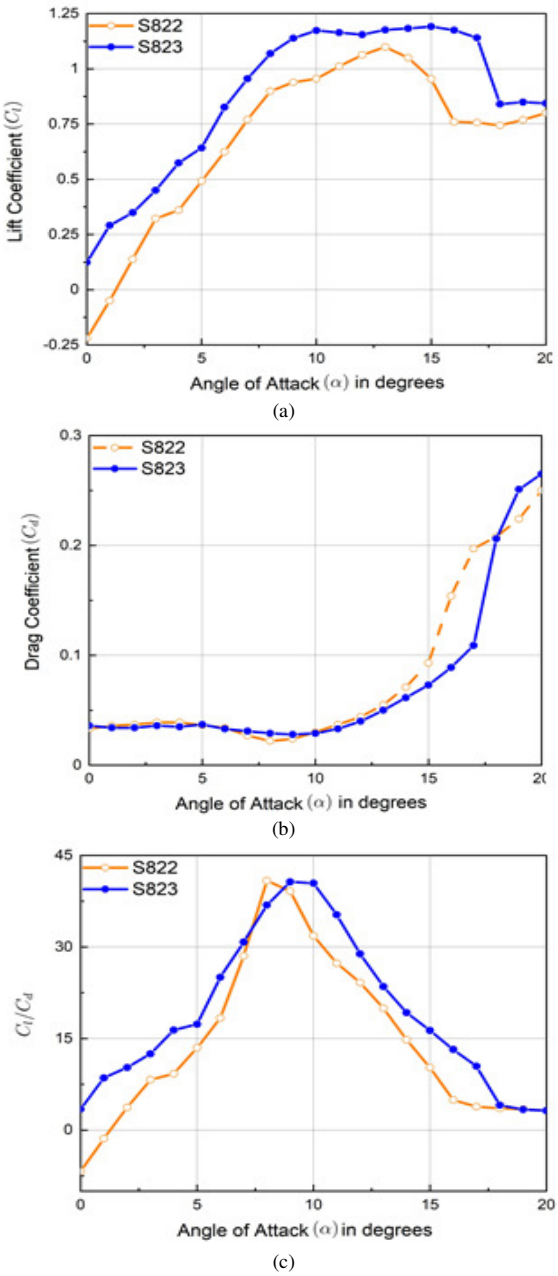

Fig.3 Aerodynamic characteristics of S823 and S822 airfoils at Re = 100, 000

D. Design of Rotor Blade

Achieving efficient blade geometry is not a straightforward process that can seldom be achieved in a single step, rather it is an iterative process involving several substeps. The design of a rotor blade is governed by the principles of aerodynamics that can be comprehended in Blade

Element Momentum theory (BEMT) as articulated in [19]. In this heuristic process, three blades are achieved under three different operating conditions. Initially, an ideal blade presented in figure 4a is obtained under the non-influential effects of wake rotation (ω), drag (C_d), and tip losses (F_i). Under this condition, the ideal blade exhibits geometry with large sectional chord and twist distributions as presented in figure 4a. An ideal blade is difficult to manufacture owing to the large geometrical variations in the blade. Nevertheless, it acts as the starting point in the blade design process leading to much efficient designs.

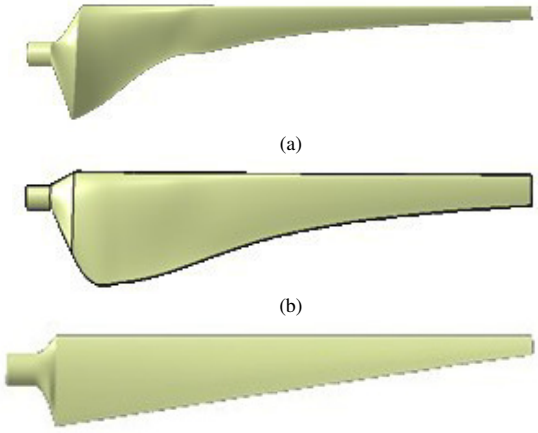

(a)

(b)

(c)

Fig.4 Geometries of Ideal, Semi-Ideal and Linearized Blades

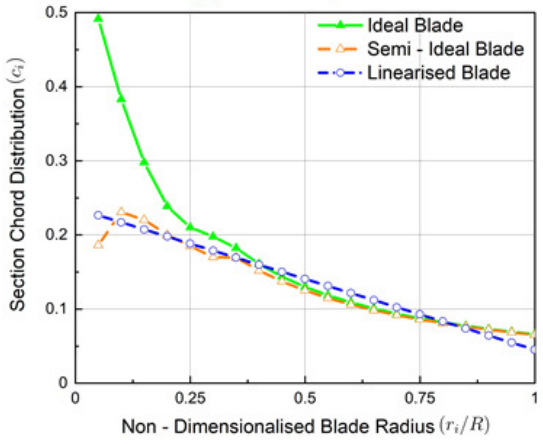

(a)

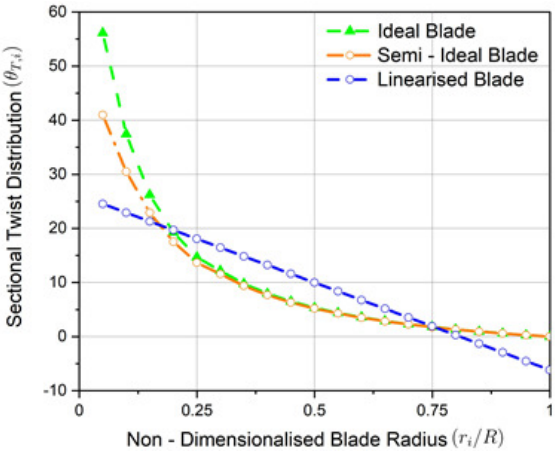

(b)

Fig.5 Sectional chord and twist distribution for Ideal, Semi-Ideal and Linearized Blades

In the second iteration, blade design is accomplished from a more realistic perspective considering the apparent effects of wake rotation (ω) and coefficient of drag (C_d). This changes the local chord (c_i) and twist distribution ($\theta_{T,i}$) as seen in figure 4b especially at the root section of the blade. However, manufacturing such blades will still be challenging due to the large geometry manifested at the root of the blade. A blade with abrupt and discontinuous geometry requires specialized manufacturing techniques. The cost incurred for fabricating such blade will become tremendously high and increase the overall cost of the blade or the wind turbine system itself [38].

To prevent the escalation of costs and at the same time to produce highly efficient albeit slightly lesser than the ideal or the semi-ideal blades, most of the wind turbine manufacturers opt for linearization technique. Linearizing the blade profile is the last step in the design of a more realizable blade for a horizontal axis wind turbine. Linearizing the blade profile leads to a simpler geometry that eases the manufacturing complexity and eventually reduces the cost of production of the blades [38]. In the present work, an effective two point scheme MATLAB code has been used to linearize the chord and twist angles of the optimized blade [39]. Linearization of the blade profile is elucidated by a

single degree polynomial expression as demonstrated by the equation $f(x)=p_1x + p2$, where, p_1 and p_2 are constants obtained from the graphical values. The MATLAB code projected a simple linear curve of best fit by optimizing the slopes of the chord $c_i$and twist angles $\theta_{T,i}$ at multiple radial locations of the blade. Figure 4c clearly shows the linear blade with simpler chord and twist distributions from the root to the tip as compared to other two blades. Henceforth, only the linearized blade will be considered in all the forthcoming analysis.

III. NUMERICAL STUDIES

In this section, methodology used for numerical studies on the model, whose analytical results have been provided in the previous section, is demonstrated.

E. Geometry and Fluid Domain

For the present study, one single wind turbine blade with 120^o hub and nose cone dissection is considered for simulation. The dimensions of the domain encapsulating the blade are shown in fig. 6.

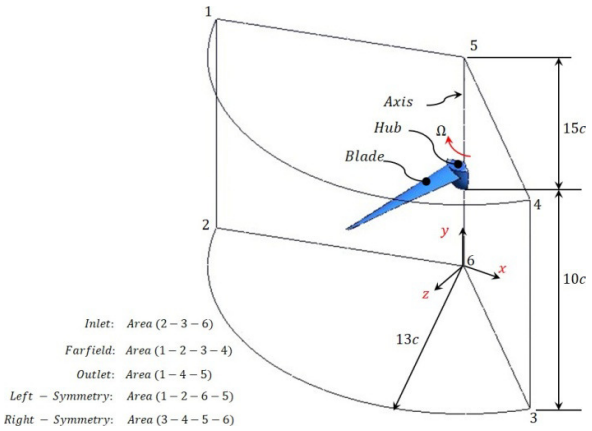

Fig. 6 Computational domain with dimensions finalized for the rotor blade

F. Mesh details

To make computation faster, cut-cell technique of mesh generation is employed in the study. Figure 7shows the grid generated for 1/3rd model and the closer look at the blade indicates the cell adaption along the blade-hub as well as hub-domain interfaces.

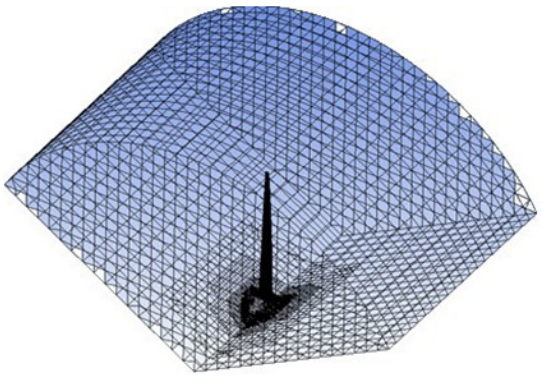

(a)

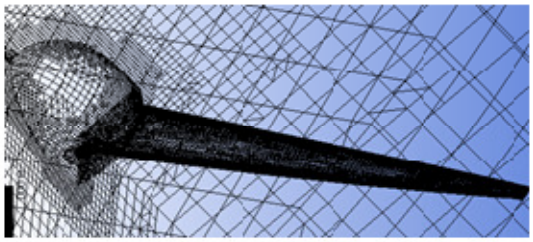

(b)

Fig. 7 Illustration of meshing of blade with the computational domain

G. Solver details

Since the flow is low-speed subsonic, there is hardly any density gradient in the flow, rendering the study to be incompressible. While, there is considerably larger role of the viscous forces in the flow domain leading to vortex formation. The meshed fluid domain is subjected to boundary conditions. As the transient studies are initial boundary value problems, the study is accompanied by initial guess generated by solving the problem for steady conditions during the first 200 iterations, which is then switched over to transient condition. For the study, Pressure Based Navier Stokes (PBNS) solver with k–ω SST model is considered. Spatial discretization is set to second order for turbulent kinetic energy and dissipation rate. The transient

formulation is set to second - order implicit and the residue is monitored within 1e-3. The relaxation factor is specified as 1 and 0.9 for turbulent kinetic energy (k) and dissipation rate (ω) respectively. The turbulent viscosity ratio and turbulence intensity at inlet and outlet boundaries are specified to be 1 and 1% respectively.In the study, RANS approach is used as the turbulence model to solve for the boundary conditions specified.The idea behind the RANS equation is Reynolds decomposition. Reynolds decomposition is a mathematical technique used to separate the time averaged and fluctuating quantities of the flow as given by equation 2.

$$\rho\overline{u}_j\left(\frac{\partial\overline{u}_i}{\partial x_j}\right)=\frac{\partial\overline{p}}{\partial x_i}+\mu\frac{\partial}{\partial x_j}\left[\frac{\partial u_i}{\partial x_j}+\frac{\partial u_j}{\partial x_i}\right]-\frac{\partial}{\partial x_j}\left(\rho\overline{u_i'u_j'}\right) \quad (2)$$

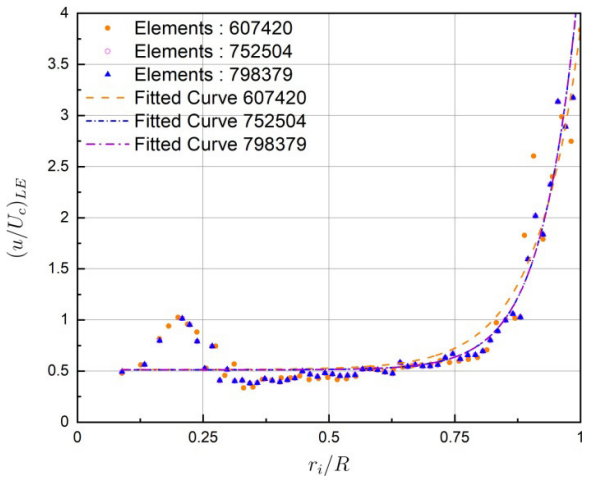

Fig. 8 Results of mesh independence of the blade

Upon setting the solver parameters, the solution is obtained for different grid sizes to check for grid independence. In total, the analysis was run for 6 different mesh sizes out of which only three are shown in figure 8. For checking for mesh independence study, further, the local velocity (u) along the leading and trailing edge of the blade is non-dimensionalised by considering themaximum velocity (U_{max}) along the edges. The variation of the non-dimensionalised velocity is plotted against the non-dimensionalised length of the blade (ri/R)along the leading edge as indicated in figure 8. It can be observed that curves for mesh with 752504 and 798379 elements almost coincide, indicating negligible influence of the mesh on the result. Based on the aboveobservations, for all the further studies, mesh with 798379 elements is selected.

IV. NUMERICAL RESULTS

H. Estimation of blade performance

The torque and power generated by the linearized blade at the operating velocities ranging from 1–20m/s are shown in figure 9. The linearized blade manifests a parabolic increase in torque and power with the wind velocity. Torque of the linearized blade recorded a meagre finite non-zero value of 0.495Nm at 1m/s. As the wind velocity increases, the torque generated by the linearized blade too increases rather in a more quasi-linear manner. At design velocity U_∞=10m/s, the blade developed a torque equaling 48.480Nm and at U_∞= 20m/s it reached 197.921Nm.

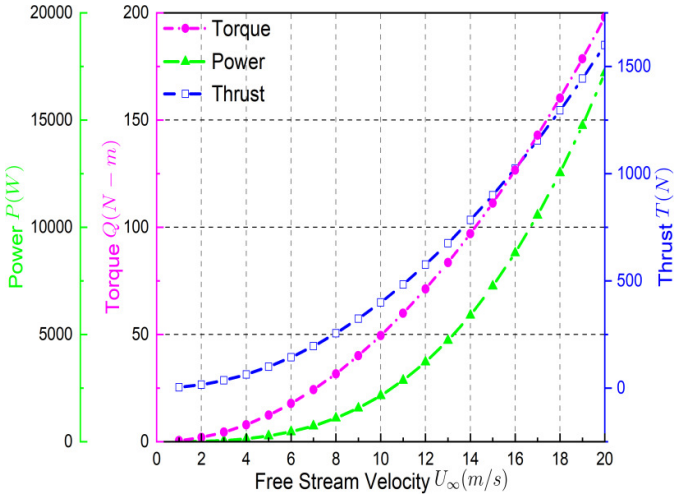

Fig. 9 Performance characteristics of the rotor blade

Since mechanical power P is a product of torque Q and angular velocity Ω, the power output of the rotor blade increases with the cube of wind velocity U_∞. With every increase in wind velocity, the power is seen to increase linearly especially up to U_∞=6m/s. Later, the power curve is seen to raise more dramatically registering higher values due to the increase in torque which is affected by the wind velocity. Beginning with 2.15Watts of power at U_∞=1m/s, it reached to 2049.98Watts at design

velocity i.e., U_∞=10m/s. Further, the power rose very quickly at higher velocities and registered a maximum mechanical power of P=17199.869Watts at 20m/s. The power trend is seen to be more pronounced at higher velocities as compared to low velocities.

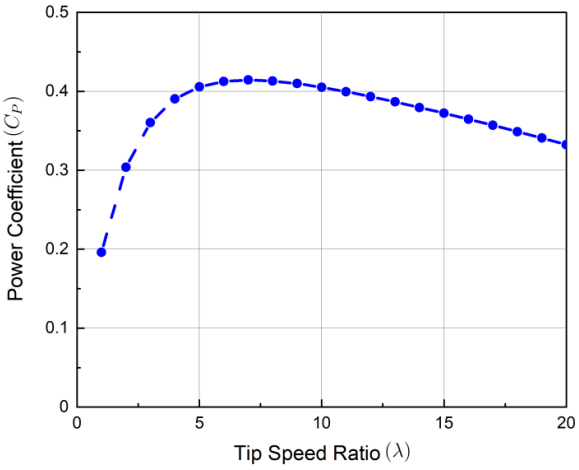

Fig.10Variation of Power Coefficient of the linearized blade

The coefficient of power C_p corresponding to the power output of the blade at various tip speed ratios λ is depicted in figure 10. The C_p–λ trend depicted in the figure is similar to the trend of any typical wind turbine and this confirms the positive outcome of the analysis. The coefficient of power C_p at λ=1 is ascertained to be 0.20. Raising the wind velocity and the proportional tip speed ratio shows that the C_p increases linearly till the TSR equals 3. When the TSR is graduated beyond λ=3, $C_p$increases albeit with slight deviation from linearity. The Cp non-linearly increases until λ=7 where the highest manifestation of $C_{p=}$0.4134 is achieved and hence the maximum $C_p$expressed by the linearized blade occurs at λ=7. Marching ahead the $C_p$starts to reduce gradually from λ=7. Through the rest of the TSR analyzed, the reduction in $C_p$is seen to happen in a more linear fashion with a constant slope as evidenced from the figure. Finally, the $C_p$ceases to the lowest value of 0.3324 at λ=20.The results obtained from the numerical studies are consolidated to identify few characteristics. Figure 11 indicates the variation of non-dimensional velocity given in equation 3 with non-dimensional blade radius.

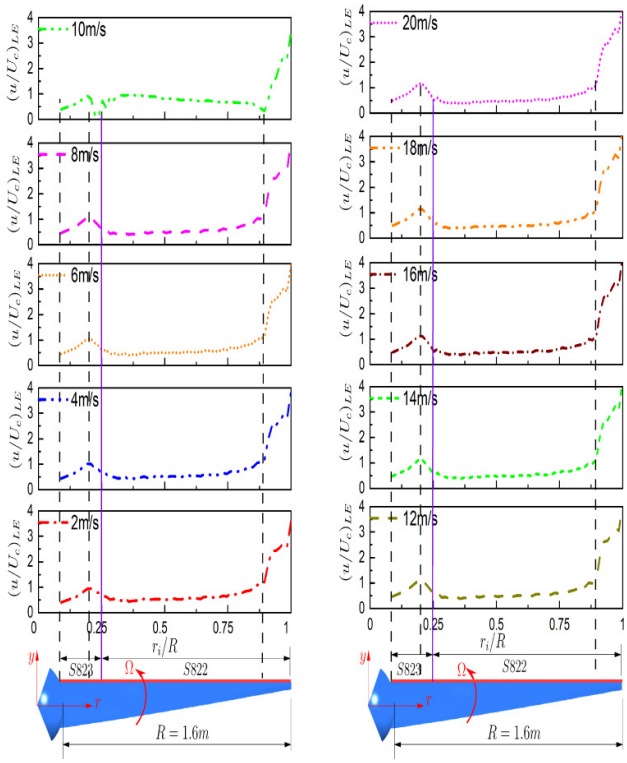

(a) 2m/s < U∞ < 10m/s (b)12m/s<U∞< 20m/s

Fig 11 Variation of non-dimensionalised velocity from root to tip of the blade along the leading edge forU∞ varying from 2m/s – 20m/s

$$Uc = 2\overline{U} / \sqrt{\pi} \tag{3}$$

Non-dimensionalised velocity is x= u/U_c , which is plotted against the non-dimensionalised length r_i/R for leading edge (fig. 11a, fig.11b) and trailing edge (fig.12a, fig. 12b). From the plots, it can be observed that the influence of the hub can be found up to 13% of the blade length. The flow over the hub decreases the pressure at the blade hub, thereby increasing the local velocity. Also, at the tip, a similar behavior is observed where the wing-tip vortices have a greater influence on the spanwise velocity profile. The effect on the upper surface is up to a length of ≈ 13% from the tip of the blade, whereas on the leeward side of the blade it is quite

negligible with a value of ≈ 5%. This might be due to the reason that the spanwise flow and the chordwise flow interact at the tip with the flow trying to move towards the upper surface (windward side) before separating from the wing in the form of vortex. When the flow moves to the upper surface, the influence on the leeward side is reduced causing lesser effect. This phenomenon has a detrimental effect on the torque produced.

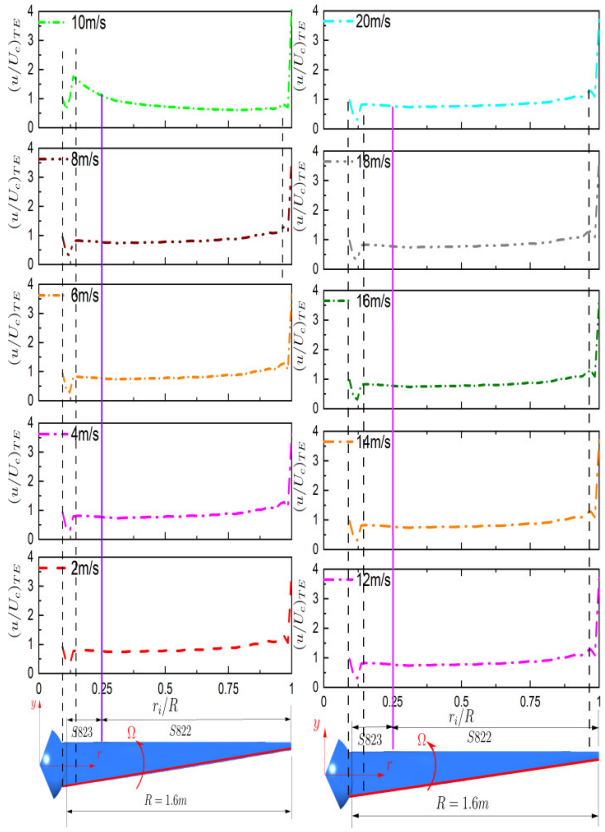

(a) 2m/s < U∞ < 10m/s (b) 12m/s < U∞ < 20m/s

Fig 12 Variation of non - dimensionalised velocity from root to tip of the blade along the trailing edge forU∞ varying from 2m/s – 20m/s

The torque values obtained for the free stream velocities U_∞=2-20m/s through the numerical approach is presented against the analytical values in figure 13a. It is evidently clear from the comparative graph that the numerical values for the entire range of test are agreeing supremely well with the analytical BEM outcomes. The agreement between the numerical and analytical values is further supplemented by the error plot presented in figure 13b. From the graph, the error is somewhat slightly accentuated especially at 2 and 4m/s. With increment in velocities the error tends to reduce and at moderate and high free stream velocities, the numerical values overlap with the BEM values. The error graph also proves that the numerical methodology implemented in the study is quite satisfactory.

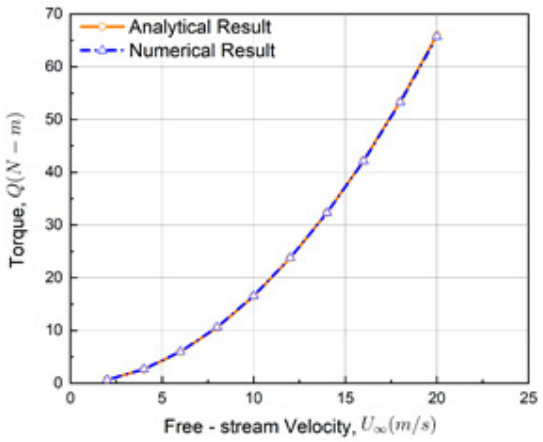

(a) Comparison of analytical and numerical results

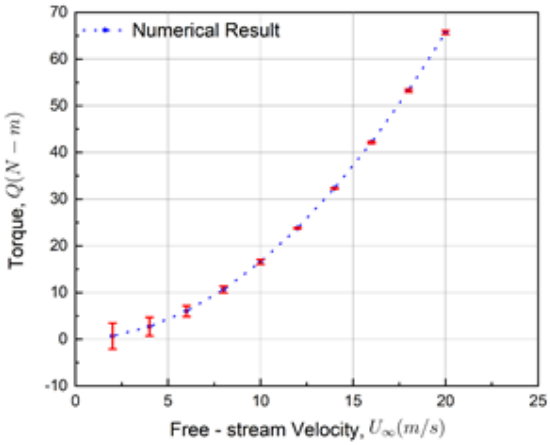

(b) Error plot for numerical results

Fig 13Comparison of analytical and numerical torque for the blade

Finally, the power P and power coefficient C_p achieved through ANSYS simulation is graphically compared with BEM results in figure 14a and b. Similar to the torque trend, the variation in power generated by the rotor blade ascertained through ANSYS is in unison with the BEM values. A slight

albeit an insignificant error in numerical power values are seen to be obtained at velocities 2m/s and 4m/s. However, the difference between the numerical and BEM power output was less than 3%.

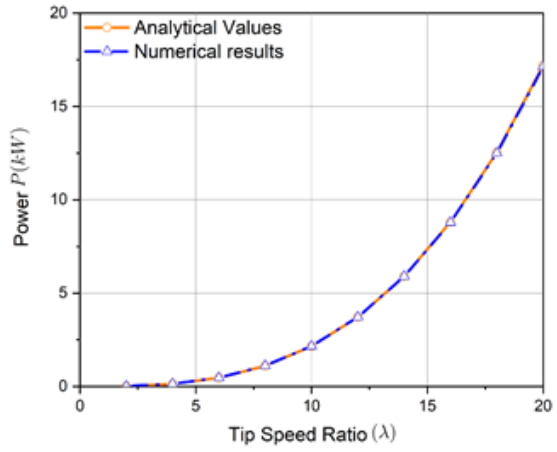

(a)

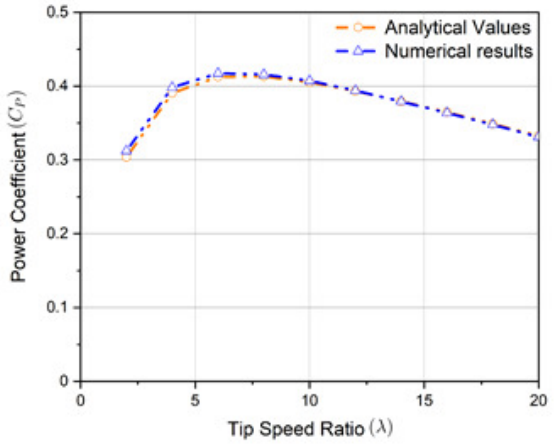

(b)

Fig 14Comparison of analytical and numerical power and power coefficient for the blade

The figure of merit for any wind turbine manifested by power coefficient C_p for both BEM and numerical approaches are illustrated in figure 14b. A slight deviation in torque values obtained through numerical approach is again reflected in the power coefficient curve. Nevertheless, the coefficient of power C_p curve is very much similar to the analytical trend. The consensus between BEM and numerical values again positively confirms the numerical torque and power values. As per the formula $\lambda=\Omega R/U_\infty$, for R=1.6m and U=10m/s, the theoretical TSR was recorded to be 6.98 that can be approximated as $\lambda=7$ at design condition. As per the numerical outcomes, the maximum $C_p=0.4182$ was yielded at TSR $\lambda=7$, whereas the theoretical outcome was $C_p=0.4134$ giving out an error of 1.16% at design conditions. Beyond $\lambda=7$, the rotor blade depicted a gradual decline in coefficient of power C_p as seen in the plot.

V. DISCUSSION OF THE RESULTS

Through ANSYS numerical simulation large variety of information can be extracted. The results can be aerodynamic forces, thrust, torque, power, pressure distribution, wake etc. But to comply with the objectives of the study, we restrict to only torque and power information of the rotor blade.

The torque, power and the corresponding power coefficient computed from BEM analysis at U_∞=2-20m/s is presented in figure 9. The analytical BEM results are used to validate the numerical outcomes of the performance of the rotor blade obtained using k-ω turbulence model in ANSYS. Analytical and numerical Torque presented in figure 9 shows good agreement at most of the wind velocities. Torque, is defined as a product of force and the radial distance. Movement of air over the blade surface causes the generation of mechanical forces like lift, drag, thrust and torque. Due to the virtue of underlying geometrical profile, the blade surface aids in generating the stated forces albeit in different directions. It is understood that the strength of aerodynamic forces depend directly on the free stream velocity U_∞, surface area S. At U_∞=2m/s, since the velocity is low, the torque of the blade arising from the low lift force is also low. With gradual increments in velocity, the lift forces tend to increase that escalates the total torque output of the blade. It can be seen from the figure 13 and 14, as the wind velocity increases, both torque and power proportionately shoots up. Same is the case for numerical torque as well as power too. At high velocities, superior lift forces generated by the

blade results in high torque, thus proportionately increases the power output of the blade. At design velocity, occurring at U_∞=10m/s, the forces arising from the flow velocity results a torque equalling Q=49.48N-m. For the generated torque, the On-Design power output is around 2049Watts, implying the same power output for which the wind turbine blade is designed to achieve at the design condition. Further, as power of the blade varies with the cube of velocity, the power output increases tremendously especially at very large velocities. But, this increase in power output cannot happen indefinitely. As the wind velocities are graduated beyond U_∞=20m/s, the airfoil might be exposed to large angles resulting in stalling of the blades. Consequently, phenomenon of stalling causes the airflow to separate from the blade surfaces that ceases the lift generation, thus reducing the torque and hence the power output to zero. Since the study encompasses wind velocities only up to 20m/s, this phenomenon is not reported in the study. Nonetheless this is the phenomenon encountered by any typical fixed speed fixed pitch wind turbines operating beyond the normal operating envelope.

The variation in the power coefficient C_p corresponding to the power output P achieved through BEM is provided in figure 10 and the same juxtaposed with the numerical output is illustrated in figure 14b. From figure 14b, it is seen that at low tip speed ratios, the performance of the blade is quite low. Low TSR corresponds to low wind velocities due to which the rotational angular velocities achieved by the blades will also be on the lower side. With the incremental TSR, the angular velocities of the blade surges attributing to a higher torque. Large torque imparted aid in generating good amount of power as the same can be noticed from the figure specifically when TSR λ equals the design condition where λ=7. Maximum power coefficient of C_p =0.4134 is attained at λ=7 when the free stream velocity operates at U_∞=10m/s. Again as the surging TSR tends to decrement the C_p trend and will continue to fall until the last TSR is tested.

VI. CONCLUSION AND FUTURE SCOPE

The study attempts to validate the numerical performance results of a rotor blade composed of two airfoils viz. S823 and S822 for a range of U_∞ and λ tested using the analytical BEM outcomes. The On-design and off-design numerical outcomes manifested by torque, power and power coefficient of the blade are found to be in good agreement with analytical results. The maximum error recorded from the blade power coefficient is found to be around 2%, which is quite negligible. Further, investigating the non-dimensionalised characteristic velocity across the blade suggests that hub and tip certainly influence the flow over the blade length. The effect of hub and tip were found to be nearly 13% and 5% of the blade length. Despite, these losses it was found that the numerical results were in good agreement with the analytical values, indicating the losses to be quite negligible when overall torque, power and power coefficient are taken into account. Though the present study restricts only up to numerical and analytical evaluation, the study can further be extended to experimental investigation to ascertain the performance under real flow conditions.

REFERENCES

[1] Letcher TM. WIND energy engineering: a handbook for onshore and oushore wind turbines. Academic Press; 2017.
[2] Hemami A. Wind turbine technology. Cengage Learning; 2012.
[3] Manwell JF, McGowan JG, Rogers AL. Wind energy explained: theory, design and application. John Wiley & Sons; 2010.
[4] Jiang H, Li Y, Cheng Z. Performances of ideal wind turbine. Renewable Energy 2015;83:658–662.
[5] Maalawi K, Badr M. A practical approach for selecting optimum wind rotors. Renewable energy 2003;28(5):803–822.
[6] Airfoil catalogue for wind turbine blades with OpenFOAM; 2017.
[7] Singh RK, Ahmed MR, Zullah MA, Lee YH. Design of a low Reynolds number airfoil for small horizontal axis wind turbines. Renewable energy 2012;42:66–76.
[8] Giguere P, Selig MS. New airfoils for small horizontal axis wind turbines; 1998.
[9] Zhu J, Cai X, Gu R. Aerodynamic and structural integrated optimization design of horizontal-axis wind turbine blades. Energies 2016;9(2):66.
[10] Polat O, Tuncer IH. Aerodynamic shape optimization of wind turbine blades using a parallel genetic algorithm.Procedia Engineering 2013;61:28–31.
[11] Sriti M, et al. Tip loss factor euects on aerodynamic performances of horizontal Axis wind turbine. Energy Procedia 2017;118:136–140.
[12] Zhu J, Cai X, Gu R. Aerodynamic and structural integrated optimization design of horizontal-axis wind turbine blades. Energies 2016;9(2):66.
[13] BabadiSoultanzadeh M, MehmandoostEsfahani B. Optimization of Horizontal Axis wind Turbine Airfoil by Using the Inverse Panel. European Online Journal of Natural and Social Sciences 2014;3(3 (s)):pp–161.

[14] Chen J, Wang Q, Zhang S, Eecen P, Grasso F. A new direct design method of wind turbine airfoils and wind tunnel experiment. Applied Mathematical Modelling 2016;40(3):2002–2014.

[15] Selig M, Guglielmo J, Broern A, Giguere P. Experiments on airfoils at low Reynolds numbers. In: 34th Aerospace Sciences Meeting and Exhibit; 1996. p. 62.

